Sequence–Activity Relationship of ATCUN Peptides in the Context of Alzheimer's Disease

Margot Lefèvre, Kyangwi P Malikidogo, Charlène Esmieu, Christelle Hureau

molecules

MDPI

Article

Sequence–Activity Relationship of ATCUN Peptides in the Context of Alzheimer's Disease

Margot Lefèvre, Kyangwi P. Malikidogo, Charlène Esmieu and Christelle Hureau *

CNRS, LCC (Laboratoire de Chimie de Coordination), 205 Route de Narbonne, BP 44099, CEDEX 4, 31077 Toulouse, France

* Correspondence: christelle.hureau@lcc-toulouse.fr

Abstract: Amino-terminal Cu^{II} and Ni^{II} (ATCUN) binding sequences are widespread in the biological world. Here, we report on the study of eight ATCUN peptides aimed at targeting copper ions and stopping the associated formation of reactive oxygen species (ROS). This study was actually more focused on Cu(Aβ)-induced ROS production in which the Aβ peptide is the "villain" linked to Alzheimer's disease. The full characterization of Cu^{II} binding to the ATCUN peptides, the Cu^{II} extraction from Cu^{II}(Aβ), and the ability of the peptides to prevent and/or stop ROS formation are described in the relevant biological conditions. We highlighted in this research that all the ATCUN motifs studied formed the same thermodynamic complex but that the addition of a second histidine in position 1 or 2 allowed for an improvement in the Cu^{II} uptake kinetics. This kinetic rate was directly related to the ability of the peptide to stop the Cu^{II}(Aβ)-induced production of ROS, with the most efficient motifs being HWHG and HGHW.

Keywords: ATCUN peptide; copper; reactive oxygen species; kinetics

Citation: Lefèvre, M.; Malikidogo, K.P.; Esmieu, C.; Hureau, C. Sequence–Activity Relationship of ATCUN Peptides in the Context of Alzheimer's Disease. *Molecules* **2022**, *27*, 7903. https://doi.org/10.3390/molecules27227903

Academic Editor: Gianantonio Battistuzzi

Received: 14 October 2022
Accepted: 7 November 2022
Published: 15 November 2022

1. Introduction

Alzheimer's disease (AD), the most common neurodegenerative disorder, affects more than 30 million people in the world [1] and is characterized by brain deterioration leading to problems with memory, behavior, and thinking [1,2]. According to the amyloid cascade hypothesis [3–5], the formation in the synaptic cleft of extracellular senile plaques containing high levels of copper and zinc ions embedded in supramolecular assemblies of the amyloid-β peptides (Aβ) occurs in the AD-affected brain at early stages of the disorder [6–8]. Such metal ions can be linked to the etiology of the disease, although they are also essentials and play key biological roles when placed in different biological environments [9]. The depletion of essential copper and zinc pools caused by the sequestration in the senile plaque peptides is a main issue. Another one is due to the redox ability of copper ions that can cycle in biological medium between its cuprous (Cu^{I}) and cupric (Cu^{II}) states, thus participating in the formation of reactive oxygen species (ROS) from the incomplete reduction of dioxygen to superoxide, hydrogen peroxide, and hydroxyl radical fueled by a physiological reductant such as ascorbate [10–12]. We and others have shown that when bound to Aβ, Cu ions retain their ability to catalyze the formation of ROS, which participate in the oxidative stress observed in AD [13,14]. This is one of the reasons why Cu ions are interesting therapeutic targets in AD [15–20].

The Aβ peptide has a well-known metal-binding domain located in the first 16 residues (DAEFRHDSGYEVHHQK) of the full-length 40/42-amino-acid-long peptide [21,22]. It includes N-ligands (imidazole histidine (His) Nim, deprotonated amide N^{-}, and terminal amine (NH_2)) as well as O-ligands such as C=O from an amide bond and carboxylate groups (COO^{-}). For Cu^{II}, two main forms are in equilibrium near neutral pH, with the terminal amine, two Nim groups from the His6 and His13 or His14, and one C=O from an amide bond, more likely that of the Asp1-Ala2 bond, being bound to the Cu^{II} in the predominant form at neutral pH (Scheme 1) [23]. The Cu^{II} affinity of Aβ is about

10^9 M^{-1} at pH 7 [24]. Cu^I is linked by two imidazole groups with a preference for the His6/His13 couple [25,26], while the value of the affinity is still under debate and oscillates between 10^7 and 10^{10} M^{-1} [27,28]. In the case of Zn^{II}, the main binding site is composed of two carboxylate functions (mainly from Asp1 and Glu3) and two imidazole groups from His6 and His13 or His14 [29]. The Zn^{II} affinity of Aβ is about 10^5 M^{-1} at pH 7 [30,31].

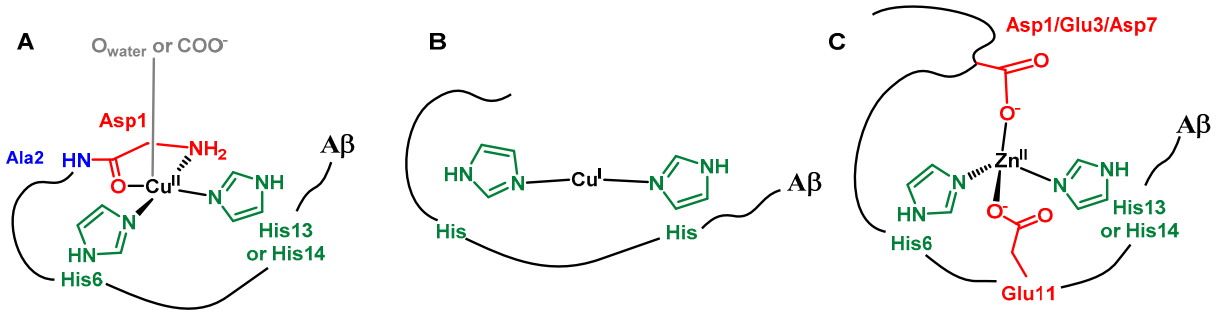

Scheme 1. Cu^{II} (**A**), Cu^I (**B**), and Zn^{II} (**C**) sites in Aβ.

Molecules that target Cu in the AD context currently represent an intense field of research. In this context, we and other research groups have focused on various chelation approaches. Highly relevant and complete reviews on this topic can be consulted by the interested reader [15,20,32]. In the present study, we focused on the use of peptide-based ligands that combined several key prerequisites with respect to further therapeutic applications, which include easily tunable Cu^{II} affinity and selectivity as well as the possibility of appending brain delivery sequences [33,34]. The sequences chosen are shown in Scheme 2. All eight of the peptides have a free terminal amine and a histidine (His) residue in the third position. This is the prototypical sequence used to create an amino-terminal copper and nickel (ATCUN) binding motif in which the Cu^{II} ion is bound by the N-terminal amine, the proximal nitrogen atom from the histidine (His), and the two deprotonated amide groups in between [35–38], as also observed in the solid state via X-ray crystallography data [39]. In such an environment, the Cu^{II} center is tightly bound with an affinity of about 10^{12} to 10^{14} M^{-1} depending on the exact sequence and with a low cathodic potential, making it resistant to reduction by the physiologically relevant ascorbate (Asc) [36]. In addition, the ATCUN motif is highly specific to Cu^{II} and Ni^{II}, as its name indicates, but not to the softer Zn^{II} ion, which has no ability to induce the deprotonation of the peptide bond. Hence, such peptides are highly specific to Cu^{II} with respect to Zn^{II}. Last, they have previously shown to be good candidates to prevent Cu(Aβ)-induced ROS production in the AD context [40–46]. However, in all but two studies [42,46], the ATCUN peptides were added when the Cu ion was exclusively in its +II state, which is not the biological reality because the brain is quite rich in Asc (about 300 μM) extracellularly [47,48].

We recently showed that when added in presence of a mixture of +I and +II states (i.e., when the Cu(Aβ) is producing ROS), the exact sequence of the ATCUN matters due to participation of Cu^{II} complexation kinetic issues [46]. Within the same context, the importance of such kinetic parameters was previously demonstrated in case of aza-macrocyclic ligands [49]; this originates from the competition between the Cu^{II} removal from Cu^{II}(Aβ) by the studied ligand to form a redox stable Cu^{II}(ligand) complex and the reduction of Cu^{II}(Aβ) to Cu^{I}(Aβ) by ascorbate.

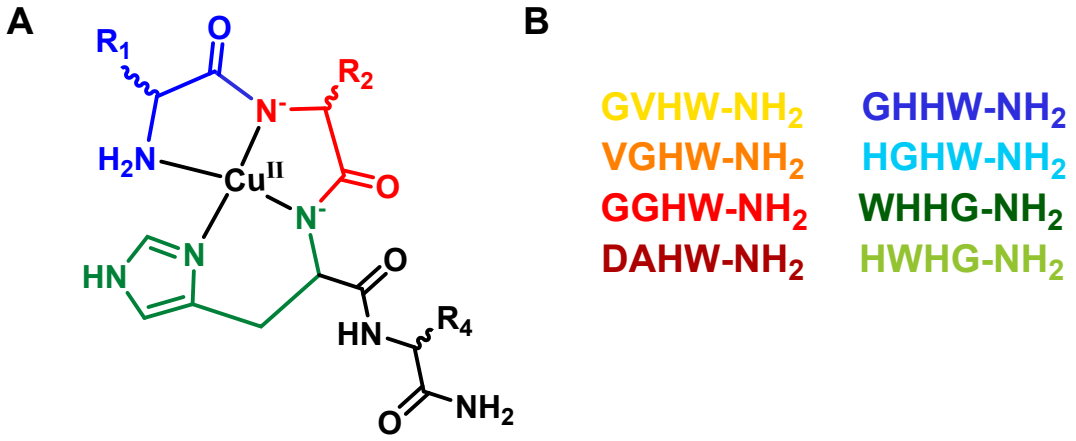

Scheme 2. Schematic representation of the Cu^{II}(P) ATCUN coordination site (**A**) and sequences of the peptide studied in the present work with the color code used thereafter (**B**). $R_{1\text{-}4}$ corresponds to the side chain of the amino acid residues; position 3 (green residue in Panel (**A**)) is His by definition in an ATCUN peptide.

In the present work, our main objective was thus to reveal some of the key features that the ATCUN sequences should have to be as appropriate as possible with respect to such kinetic issues. In the series of the eight peptides studied (Scheme 2B), several parameters were varied; the main one was the number of His: one or two. Indeed, based on recent results, the addition of a second His was expected to accelerate Cu^{II} binding and the removal from Aβ and to help the coordination of Cu^{I} in a site close to the one observed in Aβ (Scheme 1). For one-His-containing sequences, we tested the effect on steric hindrance by varying the two first residues: GGHW (red), GVHW (orange), and VGHW (yellow). For two-His-containing peptides [36,41,46,50,51], we varied the position of the second His (in position 1 or 2) and the position of the Trp residue, resulting in the following four: HGHW (light blue), HWHG (light green), GHHW (navy blue), and WHHG (dark green). In addition, we used the DAHW peptide as a reference because the DAH sequence is found in human serum albumin and has thus been extensively studied [35–38,52,53]. All of the peptides were amidated at the C-term. A Trp residue was added to monitor the Cu^{II} binding and Cu^{II} removal from Aβ at a concentration in the μM range [54,55], thus closer to the physiological range than the classical concentrations used for spectroscopic monitoring via UV–vis and EPR (in the low mM range). Lastly, note that we used the DAEFRHDSGYEVHHQK sequence (later noted as Aβ for matter of simplicity) isoform, which does not aggregate like the full-length peptides, but as stated previously, retains the metal-binding properties [21,22] and is thus appropriate to study events linked to $Cu^{II/I}$ coordination such as those reported in this work.

First, the spectroscopic and electrochemical descriptions of the Cu^{II} site in the eight ATCUN peptides and the determination of their rates to remove Cu^{II} from Aβ will be reported. Then, we will show that the two-His-containing peptides were the most appropriate to stop Cu(Aβ)-induced ROS production, with HGHW and HWHG regarded as the most promising due to their faster Cu^{II} extraction rate from Aβ. The study of the tryptophan fluorescence quenching using copper was innovatively employed and correlated with the ability of peptides to stop Cu(Aβ)-induced ROS production.

2. Results and Discussion

2.1. Cu^{II} Binding by the Peptides and Removal from Aβ

The eight ATCUN peptides (referred to as P thereafter) were prepared according to standard solid-phase peptide synthesis (SPPS) procedures on a Rink amide resin following a general synthetic route. Details of peptides synthesis and characterizations are given in the experimental section and Supplementary Materials.

The eight Cu^{II}(P) complexes were characterized using UV–vis (Figure S1) and EPR (Figures 1 and S2) spectroscopies; the characteristic parameters are listed in Table 1. The eight complexes had the spectroscopic fingerprints of Cu^{II}(ATCUN) complexes; i.e.: (i) a d-d transition near 520 nm with a molar extinction value (ε) of about 100 M^{-1} cm^{-1}; and (ii) g-values of about 2.18 ($g_{//}$) and 2.05 ($g_{\perp}$) and an $A_{//}$ of about 220 10^{-4} cm^{-1} [35–39]. The recorded EPR spectra were classical for mononuclear square planar complexes with 4N coordination and had $g_{//}$ values higher than $g_{\perp}$, characteristic of an elongated Jahn–Teller distortion around the Cu^{II} center. Moreover, superhyperfine lines in the perpendicular region also indicated N equatorial ligands and were reminiscent of Cu^{II} bound in a ATCUN motif [35–39]. These measurements showed that the variations in the ATCUN sequence did not change the first coordination sphere around the Cu^{II} ion but did affect the second sphere, as some minor but relevant changes were observed, especially via EPR (compare, for instance, the spectra of the Cu(GGHW) and Cu(HWHG) complexes, which were less and more sterically burdened, respectively). More precisely, while the $g_{//}$ values remained virtually identical (within the error bar of the measurements), the $A_{//}$ value was increased for the 2-His-containing Cu(P) complexes. This was reminiscent of what has been reported for β-alanine-containing ATCUN [56] or cyclic ATCUN [57] Cu^{II} complexes. It is worth noting that for the GHHW and WHHG peptides, the coordination site composed of three nitrogen atoms (noted 3N) from the N-terminal amine, the imidazole (Im) ring forming the second His, and the deprotonated amide in between was not detected here, in contrast to previous reports on Cu^{II} binding by AHH-COOH peptides [46,51,58]. This may be linked to the amidation of the C-term carboxylate in the present case, which decreased the pH of interconversion between the 3N and 4N (that is to say, ATCUN) coordination modes, in line with the data reported on AHH-$CONH_2$ [58].

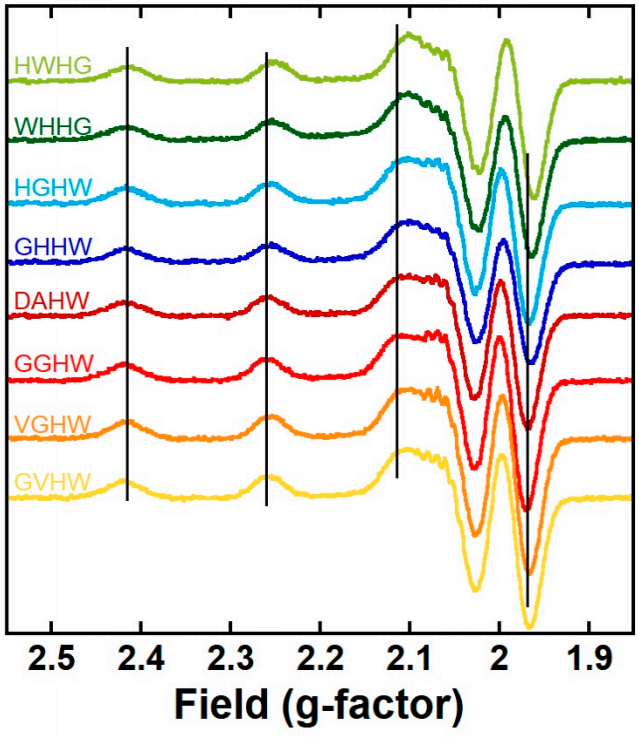

Figure 1. Low-temperature (120 K) X-band EPR spectra (second derivatives of the absorption) of Cu^{II}(P): GVHW (yellow curve), VGHW (orange curve), GGHW (red curve), DAHW (dark red curve), GHHW (dark blue curve), HGHW (light blue curve), WHHG (dark green curve), and HWHG (light green curve). The grey vertical lines follow the parallel transitions for the Cu^{II}(GGHW) complex arbitrarily chosen as the internal reference. Experimental conditions: [$^{65}Cu^{II}$] = 500 μM, [P] = 500 μM, [HEPES] = 50 mM, pH 7.4, 10% (*v*/*v*) glycerol as a cryoprotectant, T = 120 K, ν = 9.5 GHz, mod. ampl. = 5 G, microwave power = 5 mW.

Table 1. UV–vis and EPR parameters of the Cu(P) complexes.

Peptide	UV–vis		EPR [a]	
	λ_{max}	ε(M^{-1} cm^{-1})	$g_{//}$	$A_{//}$ (10^{-4} cm^{-1})
GVHW	523	92	2.18 ± 0.05	217 ± 2
VGHW	517	96	2.18 ± 0.05	217 ± 2
GGHW	524	96	2.19 ± 0.05	212 ± 2
DAHW	524	97	2.18 ± 0.05	214 ± 2
GHHW	520	89	2.18 ± 0.05	221 ± 2
HGHW	518	97	2.18 ± 0.05	222 ± 2
WHHG	523	103	2.18 ± 0.05	219 ± 2
HWHG	517	108	2.18 ± 0.05	221 ± 2

[a] The g values were calculated using the average position of the second and third hyperfine lines, while the hyperfine coupling values correspond to the field differences between the second and third line to minimize second-order contributions to hyperfine splittings. ^{65}Cu isotope was used.

The Cu^{II}(P) complexes were also studied using cyclic voltammetry (CV) (Figures 2, S3 and S4). In the cathodic scan, no processes were observed for the Cu^{II} complex made with one-His peptides; one irreversible anodic process was observed at about −1.0 V vs. SCE (−0.76 V vs. NHE) for the four Cu^{II} complexes constructed using the double-His peptides, which was in line with previously reported data [39,42,50,56,59]. For the two-His-containing Cu^{II}(GHHW) and Cu^{II}(WHHG), an additional cathodic peak was detected at about –0.5 V vs. SCE (0.74 V vs. NHE) (Figures 2 and S3). This peak was at a similar potential value to those detected for the 3N form of the Cu^{II}(AHH-COOH) complex [51] or Cu^{II}(GHK) [39] and Cu^{II}(RHDSG) [60], which adopted a 3N Cu^{II} binding site (Scheme 3C). This indicated that although it was not detected by EPR, the 3N form of the Cu^{II}(GHHW) and Cu^{II}(WHHG) complexes, in which Cu^{II} was coordinated by three equatorial ligands, the NH_2 of the N-terminus, the N of the imidazole of His, and the nitrogen of the peptide bond between AA1 and AA2 (AA = amino acid residue, NH_2, N, NIm) as shown in Scheme 3C exists in a sufficiently high amount to be reduced and observed by CV. Indeed, as the reduction of the 3N form occurred prior to that of the 4N form in such 3N/4N hybrid complexes, the electrochemical process drives the 3N–4N equilibrium to the 3N form in an electrochemical-chemical process. It was noteworthy that when the second His was in the first position instead of the second position, the CV trace was different, indicating that in the case of a "split His", as for HGHW and HWHG peptides, the analogues of the 3N form, if existing, were not in a sufficiently high amount to be detected even by CV. For all Cu^{II}(P) complexes, such low cathodic potential values indicated that the Cu(P) complexes should resist to reduction by Asc (below a certain concentration).

In the anodic scan, two main processes were expected: the oxidation of the Cu^{II}(P) to Cu^{III}(P) and that of the Trp residues. None of them could be clearly observed except for Cu^{II}(WHHG) and Cu^{II}(HWHG), for which an irreversible peak at −0.6 V vs. SCE (−0.84 V vs. NHE) and 0.7 V vs. SCE (0.94 V vs. NHE) were detected, respectively; these were attributed to the oxidation of the Trp residues (Figure S4) [61]. Indeed, we mainly observed the oxidation of the HEPES buffer. Note that we decided to work in HEPES buffer for such studies instead of phosphate buffer even though it has a larger electrochemical window, since it was shown recently that phosphate ions can interact with 3N Cu^{II} species and modify their properties [62]. However, the results indicated that the Cu^{II}(P) complexes' oxidations were at values that were too high for the complexes to be oxidized by O_2.

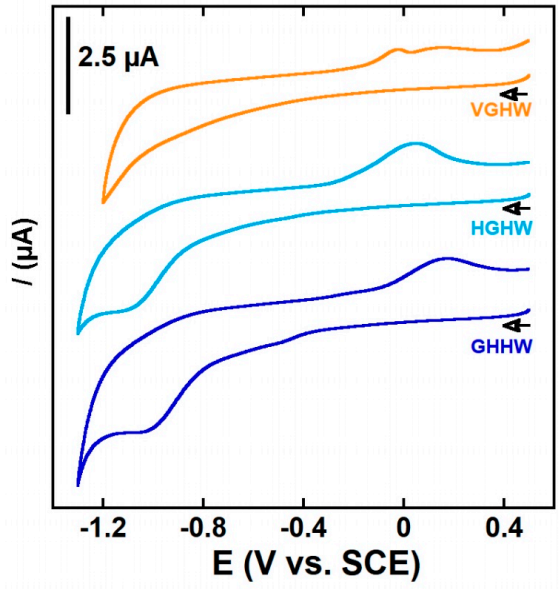

Figure 2. Cyclic voltammograms of Cu(P) with P = VGHW (orange curve), GHHW (dark blue curve), and HGHW (light blue curve); arrows indicate the scanning direction. [P] = 200 µM, [Cu^{II}] = 180 µM, [HEPES] = 100 mM, pH 7.4, scan rate 100 mV/s, T = 25 °C, working electrode = glassy carbon, reference: SCE, counter-electrode: Pt wire. E (V vs. SCE) values can be converted to E (V vs. NHE) by adding 244 mV.

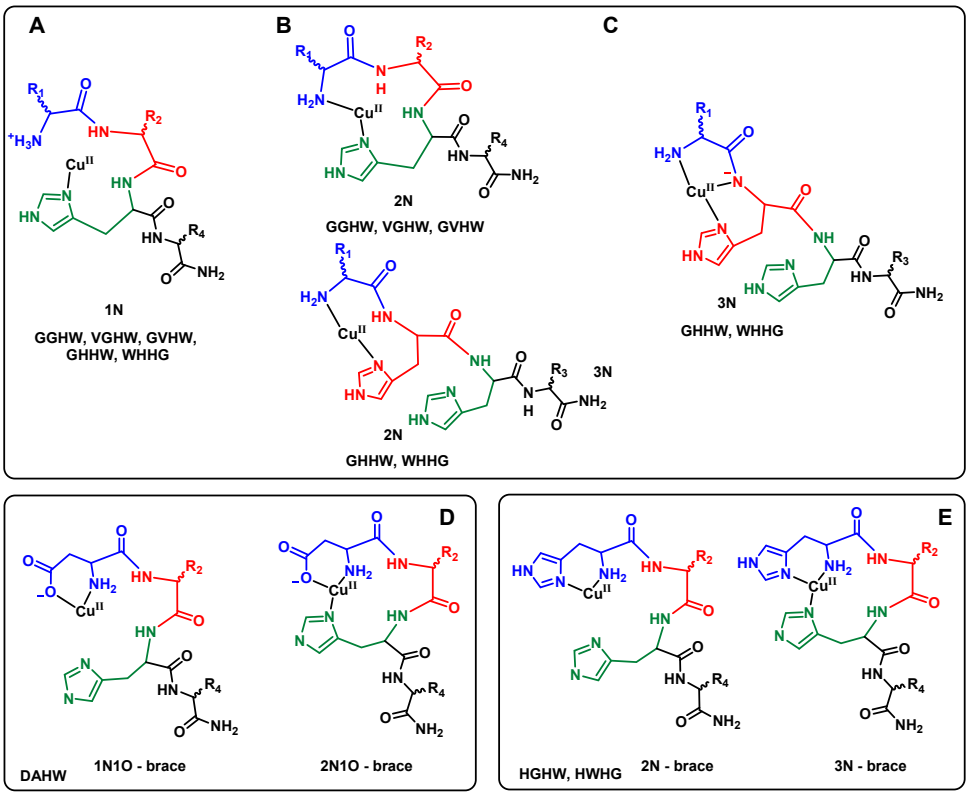

Scheme 3. Possible intermediate Cu^{II} coordination modes for the eight ATCUN peptides under study: (**A**) intermediate 1N proposed with GGHW, VGHW, GVHW, GHHW, and WHHG peptides; (**B**) intermediate 2N proposed with GGHW, VGHW, and GVHW peptides on one hand and GHHW and WHHG on the other; (**C**) intermediate 3N proposed with GHHW and WHHG peptides; (**D**) intermediates 1N1O and 2N1O proposed with DAHW peptides; (**E**) intermediates 2N and 3N proposed with HGHW and HWHG peptides. The term "brace" indicates the formation of a metallacycle.

After having shown that the peptides were all able to bind Cu^{II} and to form the corresponding ATCUN complexes, we will now describe their ability to remove Cu^{II} from Cu^{II}(Aβ). The UV–vis and EPR spectra resulting from the addition of P on Cu^{II}(Aβ) are given in Figure 3 and compared to the signatures of the Cu^{II}(P) corresponding complexes (for the one-His-containing Cu(GVHW) complex and the two-His containing Cu(GHHW); for the other peptides, see Figures S1 and S2). The UV–vis and EPR spectra of Cu^{II}(P) and P + Cu^{II}(Aβ) were superimposable for all the peptide sequences, showing the ability of all P to remove Cu^{II} from Cu^{II}(Aβ). This result was fully in line with the respective Cu^{II} affinity value of ATCUN peptides [35–39] and Aβ [24]. It is nevertheless important to note that for the one-His-containing peptides, the Cu^{II} extraction step from Cu^{II}(Aβ) was slow, in contrast to the two-His-containing peptides, which could rapidly extract Cu^{II} from Cu^{II}(Aβ); see vide infra.

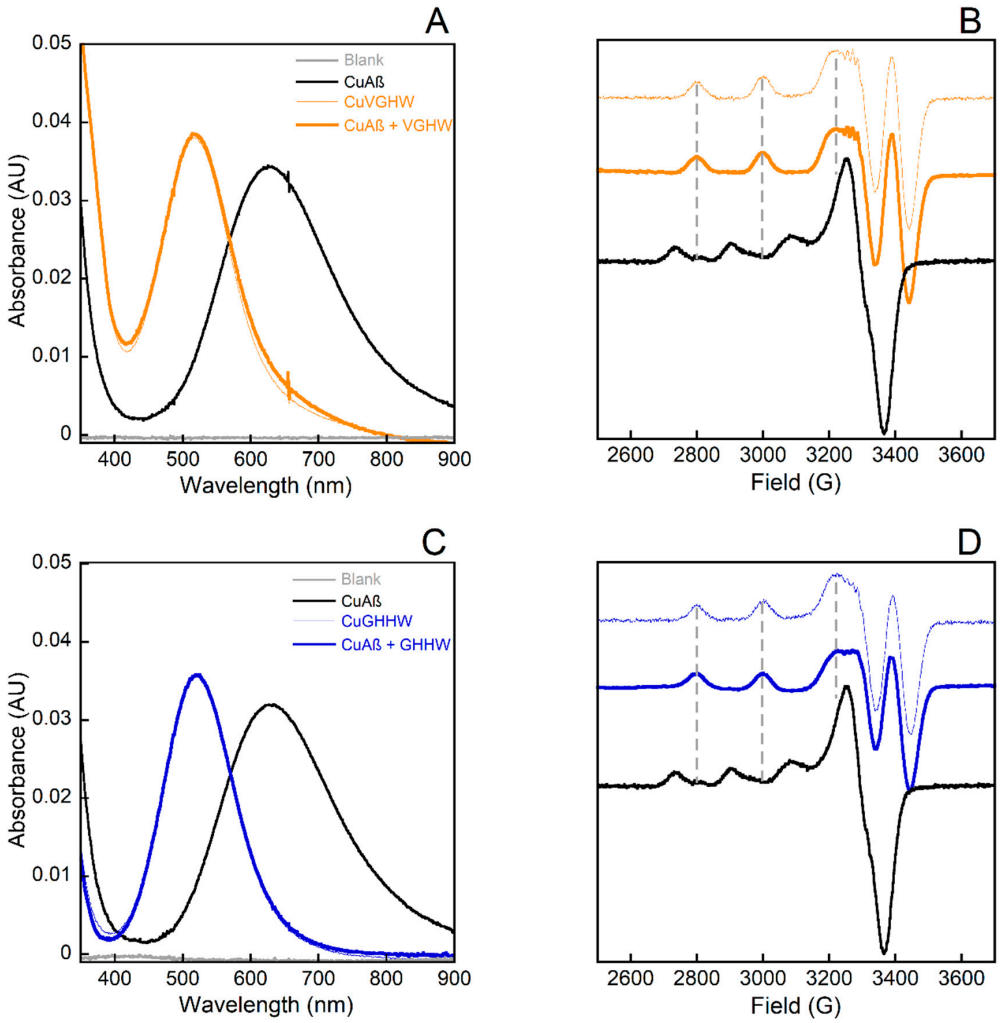

Figure 3. Cu^{II} removal from Cu^{II}(Aβ) by VGHW ((**A**,**B**) bold orange line) and GHHW ((**C**,**D**) bold blue line) followed by UV–vis (**A**,**C**) and by X-band EPR (**B**,**D**). Each panel contains spectra of Cu^{II}(Aβ) (black lines), Cu^{II}(P) (faint lines, orange for VGHW and blue for GHHW), and Cu^{II}(P) + Aβ (bold lines, orange for VGHW and blue for GHHW). The blank is also plotted in grey for the UV–vis experiments. Cu^{II}(P) + Aβ spectra were recorded after 5 min of mixing. The grey dotted vertical lines in (**B**,**D**) follow the parallel transitions of Cu^{II}P complexes as a reference. Experimental conditions for UV–vis: [Cu^{II}] = 400 μM, [P] = [Aβ] = 450 μM, [HEPES] = 100 mM, pH 7.4, T = 25 °C; for EPR: [$^{65}Cu^{II}$] = 500 μM, [P] = [Aβ] = 600 μM, [HEPES] = 50 mM, pH 7.4, 10% glycerol as cryoprotectant, T = 120 K, ν = 9.5 GHz, mod. ampl. = 5 G, microwave power = 5 mW.

Finally, the rate of Cu^{II} extraction from Cu^{II}(Aβ) by the eight peptides under study was evaluated using Trp fluorescence and its quenching when close to the paramagnetic Cu^{II} ion (Figures 4 and S5). At first glance, the experiment showed that the rate was in the following order: one-His peptides < DAHW—two-His peptides with His in positions 2 and 3 < two-His peptides with His in positions 1 and 3. Actually, a deeper inspection of the data showed that they could not be reproduced using monoexponential curves, which was in line with the presence of several processes at play (vide infra). Several observations could be made: (i) one-His peptides were slower than two His-peptides; (ii) the DAHW peptide had a faster kinetic than the other one-His peptides; (iii) among the two His peptides, those with a "split" His (i.e., HGHW and HWHG vs. GHHW and WHHG) were the fastest ones; and (iv) the position of the Trp in the double-His peptides (position 1 vs. 4 in GHHW and WHHG or position 2 vs. 4 in HWHG and HGHW) had no impact on the kinetics of Cu^{II} extraction from Cu^{II}(Aβ) by the peptides.

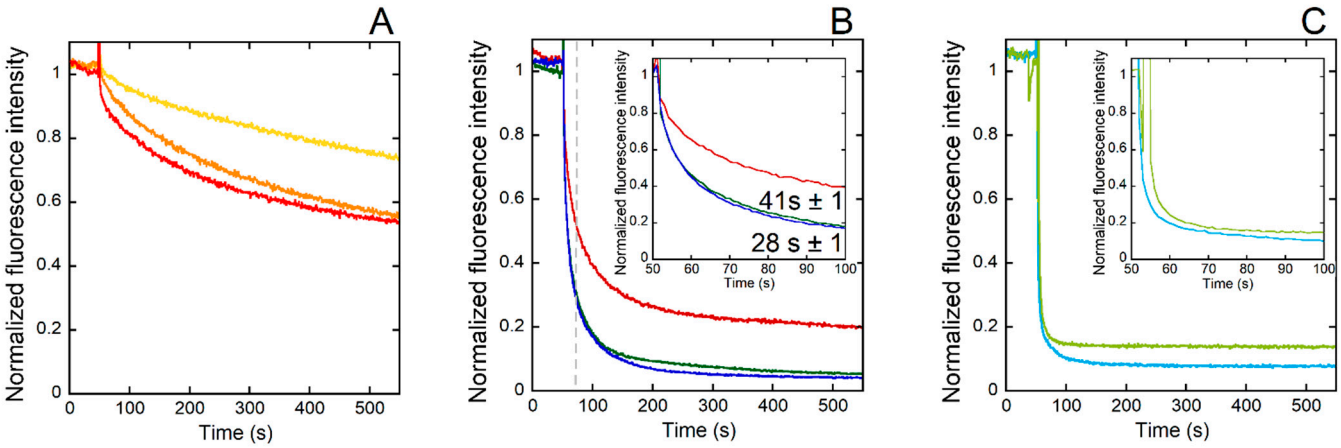

Figure 4. Kinetics of Cu^{II} removal from Cu^{II}(Aβ) by GVHW (yellow curve), VGHW (orange curve), and GGHW (red curve) (**A**); DAHW (dark red curve), GHHW (dark blue curve), and WHHG (dark green curve) (**B**); and HGHW (light blue curve) and HWHG (light green curve) (**C**) followed by fluorescence. The inset in (**B**) is an enlargement of the time between 50 and 100 s. The Cu^{II}(Aβ) was added to a peptide solution 50 s after the beginning of the kinetic. Experimental conditions: [Cu^{II}(Aβ)] = [P] = 1 μM, [HEPES] = 100 mM, pH 7.4, T = 25 °C, λ_{ex} = 280 nm and λ_{em} = 350 nm. Normalization: y = F/(Fmax-F0). In (**B**), the dotted gray line indicates when the time point corresponding to the fluorescence value from which the $t_{1/2}$ of the Cu^{II}(ATCUN) complex formation was evaluated. This fluorescence value was arbitrarily taken in order to discard the first steps in the process of Cu^{II} removal from Cu(Aβ).

These observations could be analyzed by considering several factors that influenced the two key steps in the reaction of Cu^{II} removal from Cu^{II}(Aβ): the anchoring of the Cu^{II} by the peptides leading to intermediates species and the reshuffling of the intermediates to release the Cu^{II}(P) complexes (ATCUN). Indeed, as recently thoroughly described in case of the GGH-COOH peptide [63], the formation of the Cu^{II}(ATCUN) complex proceeds via several steps that include the transformation of the 1N intermediates (anchoring via the third His residues) to 2N (binding by the N-terminal amine and the His) (Scheme 3A) to 4N (ATCUN motif, Scheme 2A) [63–65].

In the present case, we deduced that having an amino acid residue with a side chain containing donor atoms in the first position accelerated the anchoring and the formation of the intermediates. In the case of the DAHW, Cu^{II} anchoring can be proposed to occur through a 1N1O brace (Scheme 3D) and for HGHW and HWHG via a 2N brace (Scheme 3E). We hypothesized that the 2N brace is a better motif for the Cu^{II} coordination that would explain the different kinetics of Cu^{II} capture.

Among the other peptides, the GHHW and WHHG peptides were the fastest, as expected based on the literature, due to the formation of a 3N intermediate composed of

the N-terminal amine, the His side-chain in position 2, and the deprotonated peptide bond in between, as recently described for AHH-COOH (Scheme 3B) [36,46].

2.2. Arrest of Cu and Cu(Aβ)-Induced ROS Production by the Peptides

We will now study the effects of the eight peptides on Cu and Cu(Aβ)-induced ROS production. The Asc reductant fueled the reaction of incomplete dioxygen reduction to $O_2^{\circ -}$, H_2O_2, and HO° [10]. Hence, monitoring its consumption rate was an easy and robust way to monitor the formation of ROS. The concentration of Asc that fueled the reaction was followed by UV–vis at 265 nm ($\lambda_{max,}$ ε = 14 500 M^{-1} cm^{-1}). We previously showed that Asc consumption mirrors H_2O_2 formation (and to a lesser extent, HO° formation) [66,67]. Note that with respect to HO°, the correlation with Asc consumption is only qualitative because HO° is able to react with the Aβ peptide itself and thus it is not HO° formation but actually HO° release from the Cu(peptide) complex that is monitored [68,69]. Asc consumption monitoring is thus now regarded as a classical method to evaluate ROS production by $Cu^{I/II}$ complexes [41,70–72].

Three experiments were performed: (1) the addition of P to a Cu^{II} (or Cu^{II}(Aβ))-only species and then the addition of Asc to trigger the formation of ROS; (2) the addition of P after the addition of ascorbate, leading to the presence of both Cu^{I} and Cu^{II} species (or Cu^{I}(Aβ) and Cu^{II}(Aβ)) in the medium; and (3) similar to (2) but starting with Zn^{II}(Aβ) instead of Aβ. In case (1), the experiment documented the ability of P to bind Cu^{II} (or remove it from Cu^{II}(Aβ)) and to form a Cu^{II}(P) complex resistant to reduction by Asc. In case (2), not only the thermodynamic ability of P to bind Cu^{II} (or remove it from Cu^{II}(Aβ)) was probed but also the velocity at which the reaction was performed. Indeed, if the Cu^{II} binding was too slow, the reduction would proceed and the ROS would not be fully stopped. The extent of the lessening of the Asc consumption depended on the relative rates between the Cu^{II} chelation and Cu^{II} reduction reactions. In case (3) the experiments probed several key features; that is to say, the ability to remove Cu^{II} from Aβ in presence of Zn^{II} (Cu^{II} over Zn^{II} selectivity of P versus Aβ) and to form the Cu^{II}(P) (Zn^{II} impact on the kinetics of Cu^{II} removal from Cu^{II}(Aβ)).

The experiments at the Cu^{II} level (case (1)) with or without Aβ being present are shown in Figures 5A,B and S6A, respectively. In the absence of Aβ with all the peptides and with an incubation of 30 s before the addition of Asc, its consumption was fully prevented (Figure S6A). In presence of Aβ with all the peptides and with an incubation of 30 min before the addition of Asc, its consumption was fully prevented (Figure 5B). This indicated that all the peptides were able to remove Cu^{II} from Cu^{II}(Aβ) and that the formed Cu^{II}(P) species could not be reduced by Asc in such conditions, which was in line with other experiments and the electrochemical data, respectively. It is worth noting that when the incubation time was reduced to 30 s, only the two-His-containing (and to a lesser extent, the DAHW) peptides retained their ability to prevent Asc consumption (Figure 5A). This indicated that the complexation reaction was not fully completed by the other three peptides.

The experiments in which both Cu^{I}/Cu^{II} were present (case (2)) with or without Aβ being present are shown in Figures5C and S6B, respectively. The peptides behaved differently with two main trends observed: either the instantaneous arrest of Asc consumption for the four two-His-containing peptides and the DAHW; or an initial slowdown to eventually reach the basal rate of Asc consumption, with GGHW being more rapid than VGHW, which itself was more rapid than GVHW. Similar observations included the signatures of a kinetically controlled binding of Cu^{II}, which was previously observed with a nonpeptide ligand in the presence of Aβ [49,67]. In the presence of Aβ, the differences between the peptides were more pronounced, with DAHW becoming less efficient (only a slowdown in Asc consumption was observed, not a full arrest) and the other three one-His peptides being unable to arrest Cu^{II}(Aβ)-induced Asc consumption. This higher discrimination between the peptides could have two origins: (i) the time requested to extract Cu^{II} from Aβ was higher than to bind Cu^{II} due to pre-equilibrium between Aβ-bound and Aβ-unbound Cu^{II} and/or due to a more difficult anchoring for Aβ-bound Cu^{II} via the formation of

a ternary species; and/or (ii) the ratio between Cu^{I} and Cu^{II} was shifted toward Cu^{I} in presence of Aβ, leading to a weaker level of the targeted Cu^{II}. Since the relative efficiency of the peptides perfectly matched the rate of Cu^{II} removal from Aβ as measured previously by Trp-fluorescence quenching experiments, we anticipated that the first effect (i) was predominant.

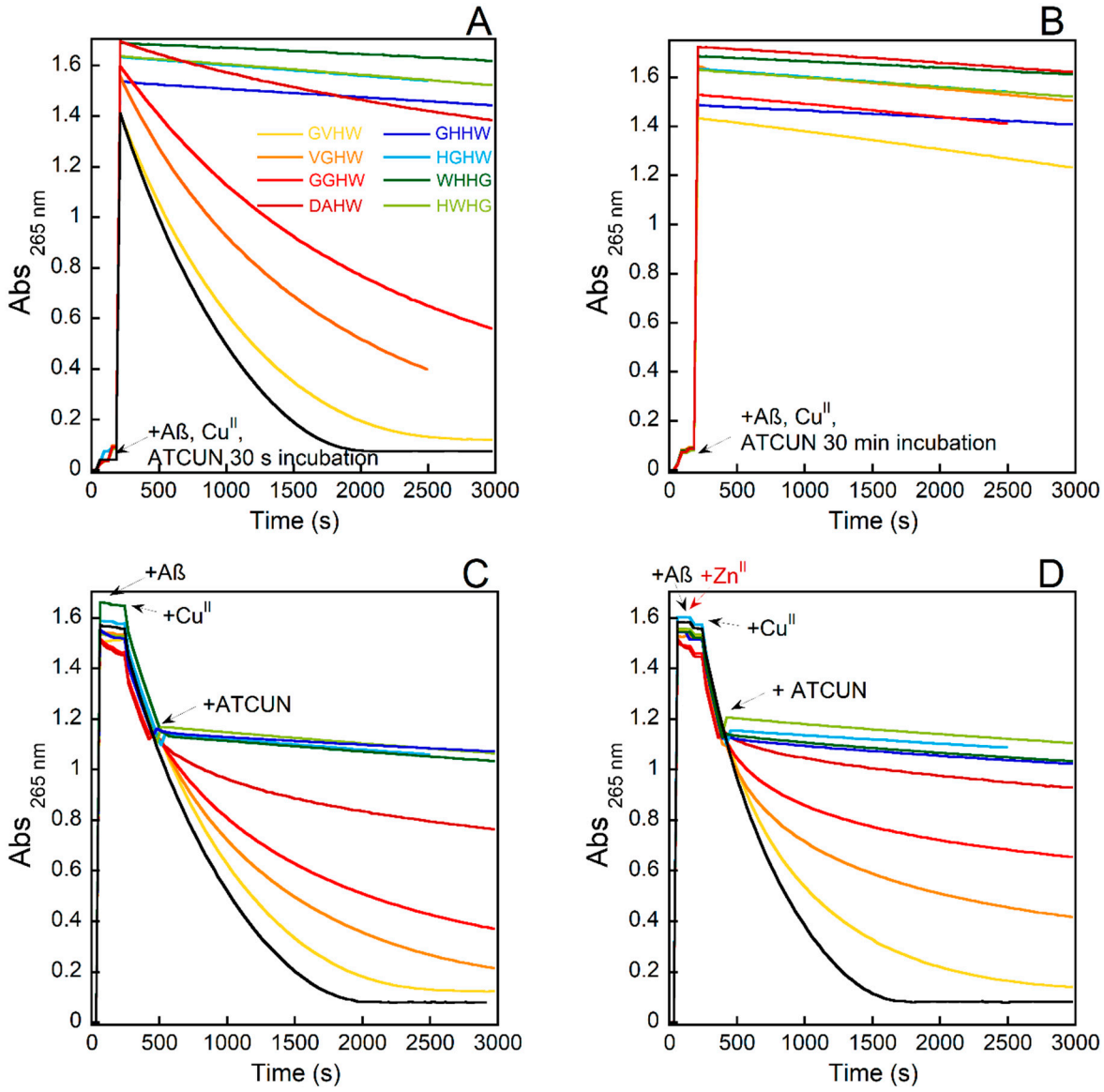

Figure 5. Kinetics of ascorbate consumption induced by Cu(Aβ) followed by UV–visible spectroscopy at 265 nm with a background correction at 800 nm starting from Cu^{II}(Aβ) with 30 s of incubation with P (**A**), Cu^{II}(Aβ) with 30 min incubation with P (**B**), $Cu^{I/II}$(Aβ) (**C**), and $Cu^{I/II}$(Aβ) in the presence of one equiv. of Zn^{II} (**D**) using GVHW (yellow curves), VGHW (orange curves), GGHW (red curves), DAHW (dark red curves), GHHW (dark blue curves), HGHW (light blue curves), WHHG (dark green curves), and HWHG (light green curves). [P] = [Aβ] = 12 μM, [Cu^{II}] = 10 μM, [Asc] = 100 μM, [HEPES] = 100 mM, pH 7.4, T = 25 °C.

In the presence of Zn^{II} (Figure 5D), the effects of the peptides were not prevented, which was in line with the relative Cu^{II}-over-Zn^{II} selectivity of the peptides and Aβ, and were even slightly improved for the one-His peptides. This may have indicated that Zn^{II} helped the Cu^{II} dissociate from the Cu(Aβ), as previously described for the parent Cu(AAH, AHH) complexes [46], thus increasing the level of accessible Cu^{II}.

A final type of experiment was performed in which the Asc consumption was triggered by the addition of air to a premixed solution containing Cu^{I} (Figure S6C) or $Cu^{I}(A\beta)$ (Figure S7) (coming from the reduction of Cu^{II} and $Cu^{II}(A\beta)$ by Asc under argon) and the peptides. Similar results to those obtained in the presence of both Cu^{I} and Cu^{II} redox states were obtained regardless of the presence of Aβ, with more pronounced differences between the one-His-containing peptides. This was in line with the higher level of Cu^{I} in this latter experiment compared to the previous one (Cu^{I}/Cu^{II} and addition of peptides during the course of Asc consumption—Figures S6B and S7).

3. Concluding Points

A first main point to be underlined is the fact that in contrast to the current paradigm, not all ATCUN-forming peptides could stop Cu-induced ROS production. When the Cu ions were engaged in the redox cycle (i.e., when Cu^{I} was present in addition to Cu^{II}), some ATCUN sequences failed to stop Cu-induced ROS production; this trend worsened in the presence of Aβ.

The efficiency of the peptides to arrest the $Cu^{II}(A\beta)$-induced ROS production perfectly followed the rate of Cu^{II} extraction from $Cu^{II}(A\beta)$. This was quite remarkable and indicated that for this series of peptides, the rate of Cu^{II} extraction from $Cu^{II}(A\beta)$ was the determinant step in the arrest of Cu(Aβ)-induced ROS production.

In Scheme 4, the two possible paths to arrest $Cu^{II}(A\beta)$-induced ROS are shown: when $Cu^{I}(A\beta)$ and $Cu^{II}(A\beta)$ were cycling, extraction of Cu^{II} from $Cu^{II}(A\beta)$ (path Cu^{II}, in pink) or from $Cu^{I}(A\beta)$ led to the formation of a Cu^{I}(peptide) complex that was oxidized to Cu^{II}(peptide) complexes, which could not be reduced back (path Cu^{I} in blue). Our data indicated that the Cu^{II} path was the one in play for the peptides studied here. This was not fully anticipated and a Cu^{I} path was first foreseen, especially in the case of the two-His-containing peptides that could compete with Aβ to bind Cu^{I}, having *a priori* the same Cu^{I} site (Scheme 1) [42,73].

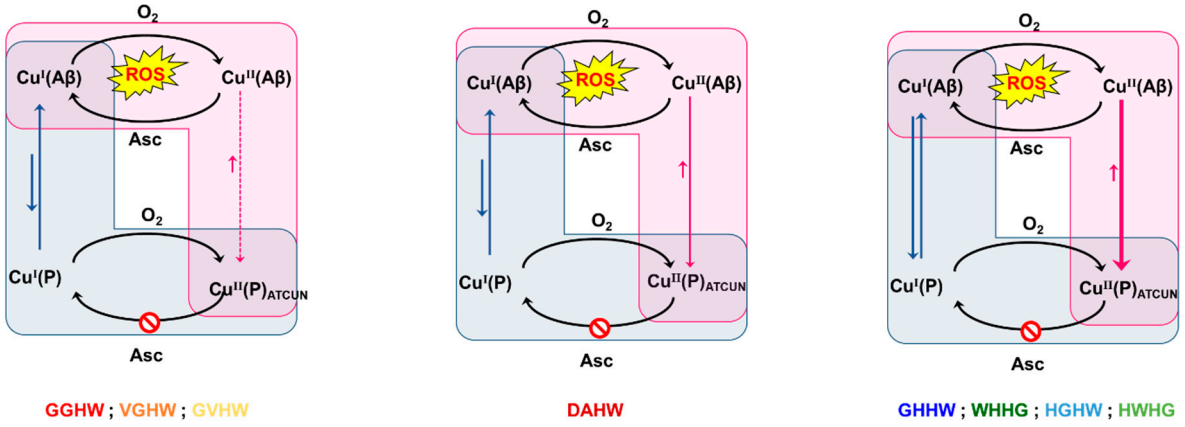

Scheme 4. The three possible routes of arrest of Asc consumption as a function of the peptides in play. In pink: the "Cu^{II} path" corresponding to oxidation of $Cu^{I}(A\beta)$ to $Cu^{II}(A\beta)$ followed by retrieval of Cu^{II} from $Cu^{II}(A\beta)$ by the peptides P. In blue: the "Cu^{I} path" corresponding to retrieval of Cu^{I} from $Cu^{I}(A\beta)$ by the peptides P followed by the oxidation of the resulting $Cu^{I}(P)$ complex to $Cu^{II}(P)$ and its rearrangement into the Cu^{II}(ATCUN) complex. Width of the pink arrows corresponds to the kinetics of the retrieval of Cu^{II} from $Cu^{II}(A\beta)$ by the peptides P. Length of arrows corresponds to the thermodynamic equilibria between the species.

The HGHW and HWHG peptides were faster in capturing Cu^{II} out of $Cu^{II}(A\beta)$ and worked perfectly in all of the experimental conditions tested in the Asc consumption assay (from Cu^{I} in the presence of Zn^{I}). The possibility of having intermediate complexes with Cu^{II} bound by the N-terminal amine and its imidazole ring side chain (thus forming a metallacycle) and by the side chain of the His in position 3 (3N-brace site, Scheme 3D),

which was reminiscent of the histidine brace LPMO binding site in Ref. [74], is proposed to be the reason why. It is also worth noting that the bulkier Trp residues in position 2 had no impact on the ability of the peptide to arrest Cu^{II}(Aβ)-induced ROS production. The quenching of the Trp fluorescence was thus a fully appropriate tool to evaluate the ATCUN motif's ability to stop Cu^{II}(Aβ)-induced ROS production. Nevertheless, for the two-His-containing peptides this technique did not allow us to probe the early steps of the Cu^{II} coordination, which were too fast to be measured. More advanced stopped-flow and freeze-quenched techniques could be used, as recently reported [63,64].

In line with previous reports [32,40,41,46], ATCUN sequences were revealed to be good candidates for further therapeutic purposes in the Cu^{II} chelation field. However, when Cu^{II}-induced or Cu^{II}(Aβ)-induced ROS are targeted, the exact sequence matters.

4. Experimental Section

All of the chemicals were purchased from Sigma-Aldrich unless otherwise specified. All of the solutions were prepared using ultrapure water (18.2 MΩ). Stock solutions of metallic salts and peptides were prepared by dissolving the salts or the peptides in ultrapure water; the concentrations were determined using UV–vis absorption spectroscopy. A stock solution of Zn^{II} ions was prepared at 100 mM using monohydrated $ZnSO_4 \cdot H_2O$ salt. A stock solution of Cu^{II} was prepared at 100 mM using hydrated $CuSO_4.5H_2O$ salt. The concentration of the solution was determined using UV–vis (λ = 800 nm corrected at 400 nm) while considering a molar extinction coefficient of 12 M^{-1} cm^{-1}. A stock solution of HEPES buffer (sodium salt of 2-[4-(2-hydroxyethyl)piperazin-1-yl]ethanesulfonic acid) was prepared at 500 mM and the pH was adjusted to 7.4 using concentrated sodium hydroxide. All pH values are given with a ±0.1 pH unit error. A stock solution of sodium ascorbate was prepared at 5 mM every two days due to its degradation in solution. The $A\beta_{1\text{-}16}$ (DAEFRHDSGYEVHHQK) peptide was purchased from Genecust (purity > 95%). A stock solution was prepared at around 10 mM; its concentration was determined using UV–vis with Tyr10 absorption considered as free tyrosine (in acidic condition, ε276−ε360 = 1410 M^{-1} cm^{-1}). The ATCUN peptides were synthetized in house and stock solutions were prepared at around 10 mM. The peptide concentration was determined by a Cu^{II} titration followed by UV–vis or tryptophane residue absorption (ε280 = 5600 M^{-1} cm^{-1}). The stock solutions were stored at 4 °C and the Aβ peptide and ATCUN peptide stock solutions at −20 °C.

Synthesis of peptides. The ATCUN peptides were synthesized using a Liberty Blue microwave peptide synthesizer with a standard 9-fluorenylmethoxycarbonyl (Fmoc) strategy on a 4-(2′,4′-dimethoxyphenyl-Fmoc-aminomethyl)-phenoxyacetamido-norleucyl-MBHA resin (Fmoc-Rink Amide MBHA resin from Fluorochem, 0.33 mmol/g loading, 1% DVB, 100–200 mesh) through solid-phase peptide synthesis protocols [75]. The coupling reactions were performed by using a 5-fold excess of amino acid, 5-fold excess of DIC, and 5-fold excess of Oxyma in DMF. The N-terminal Fmoc deprotection was carried out using 20% piperidine in DMF. Resin cleavage and side-chain deprotection were performed at the same time via treatment with 95% TFA, 2.5% H_2O, and 2.5% triisopropylsilane (TIS) for 180 min. The peptides were precipitated with cold ether from the solution after cleavage, centrifuged, dissolved in H_2O containing 0.1% TFA solution, and purified via ChromatoFlash on a INTERCHIM PURIFLASH BIO C18-T (pore size 200 Å, particle size 15 μm, 25 g) column using a gradient from 95% to 50% (*v*/*v*) of H_2O with 0.1% TFA and MeOH with 0.1% TFA. Pure peptides were lyophilized. The purity of the peptides was assessed via NMR and (+)ESI-MS.

NMR spectroscopy. The ^{1}H and ^{13}C experiments were recorded on a Bruker Avance III 400 MHz spectrometer equipped with a 5 mm broadband inverse triple-resonance probe 1H, BB (31P-103Rh)/31P with Z field gradients. All spectra were calibrated with respect to the D_2O signal (4.79 ppm). The chemical shifts (δ) are reported in ppm. The NMR coupling constants (J) are reported in Hz.

UV–visible spectroscopy. Titration and UV–vis kinetic data from the ascorbate consumption experiments were recorded with a Hewlett Packard Agilent 8453 or 8454 spec-

trophotometer at a controlled temperature of 25 °C in a 1 cm path length quartz cuvette with 800 rpm stirring.

- **Cu^{II} titration**. The peptide (P) solutions' precise concentrations were determined via Cu^{II} titration with a solution of known concentration using the d−d transition absorption of the complex to determine the equivalence point or following the λ_{max} of tryptophane at 280 nm using the molar extinction coefficient of the tryptophan (ε = 5600 M^{-1} cm^{-1}). P were titrated at 500 μM with the addition of an increasing amount of a Cu^{II} stock solution (by 0.1 eq). The UV–vis titration experiments confirmed the stoichiometry of the metal–ATCUN peptide complex at 1:1.
- **ROS experiment.** The ROS production was determined using an ascorbate consumption assay monitored via UV–vis spectroscopy. The decrease in the absorption band at λ_{max}= 265 nm of the Asc (ε = 14,500 M^{-1} cm^{-1}, corrected at 800 nm) was plotted as a function of time. The samples were prepared from stock solutions at 1 mM and mixed in situ in the UV–vis cuvette at a final concentration of 12 μM for the ATCUN peptide, $A\beta_{1\text{-}16}$, and Zn^{II} and 10 μM for Cu^{II} in HEPES at pH 7.4. Ascorbate was added to obtain 100 μM as the final concentration. The final volume was adjusted with ultrapure water to 2 mL. The ROS experiments were performed following three different procedures: starting from Cu^{II}, starting from a mixture of Cu^{I} and Cu^{II}, and starting from Cu^{I}.

For the Cu^{II} experiment, the ATCUN peptide (P) was added to the Cu^{II} or Cu^{II} + Aβ mixture, and then the ascorbate was introduced in the cuvette. Cu^{II}, Aβ, P, and ascorbate were added at 30, 60, 120, and 180 s, respectively. For some experiments, the Cu^{II} + Aβ + P mixture was preincubated for 30 min and added directly into the cuvette containing the aqueous buffered solution. The ascorbate was then introduced at 180 s.

For the Cu^{I} and Cu^{II} experiment, the ascorbate was introduced first into the cuvette; then, either Cu^{II} + P or Cu^{II} + Aβ + P or Cu^{II} + Aβ + Zn^{II} + P was added. Ascorbate, Aβ, and/or Zn^{II} and Cu^{II} were added at 30, 120, and 240 s, respectively. When the absorbance reached about 1.1 in O.D., the ATCUN peptide was added. These experiments were run under aerobic conditions.

Finally, for the Cu^{I} experiment, P was injected with a Hamilton syringe into the Cu^{I} or Cu^{I} + Aβ mixture in a sealed UV–vis cuvette under anaerobic conditions and then exposed to air (by bubbling air into the cuvette). The Cu^{I} was generated from the in situ reduction of Cu^{II} with ascorbate. All of the solutions were previously degassed for 15 min with argon before being introduced into the sealed UV−vis cuvette kept under argon.

EPR. Electron paramagnetic resonance (EPR) spectra were recorded using an Elexsys E-500 Bruker spectrometer operating at a microwave frequency of approximatively 9.5 GHz. The spectra were recorded using a microwave power of 5 mW, a magnetic field range of 2400 to 3700 G, and a modulation amplitude of 5 G. The experiments were carried out at 120 K using a liquid nitrogen cryostat. EPR samples were prepared in Eppendorf tubes from a 10 mM Cu^{II} stock solution and diluted to 500 μM in 50 mM of HEPES buffer (pH 7.4) with the addition of 500 μM ATCUN peptides. As a cryoprotectant, 10% glycerol was added. The final volume was adjusted to 200 μL using ultrapure water. The mixture was then transferred into a EPR quartz tube and frozen in liquid nitrogen.

Fluorescence spectroscopy. The kinetics of Cu^{II} chelation by the ATCUN peptides were monitored by fluorescence following the tryptophan fluorescence emissions using a Horiba Fluoromax 4 fluorescence spectrophotometer in a 2 × 10 mm path quartz cuvette with λ_{ex} = 280 nm and λ_{em} = 350 nm. The fluorescence intensity was measured using the following parameters: excitation slit: 2 nm, emission slit: 10 nm, averaging time: 0.1 s. Cu^{II} -binding kinetics that induced the tryptophan fluorescence quenching were measured via the addition of 1 eq of Cu^{II}(Aβ) to a solution of the ATCUN peptides (1 μM) in HEPES buffer (100 mM, pH 7.4) and the fluorescence monitored over time (600 s). The normalization of the fluorescence intensity was realized according to the following equation y = F/(Fmax-20,000) for comparison. We decided to take 20,000 and not the F0 because all

the curves had a different ending point and the minimum fluorescence intensity reached was 20,000 u.a. The $t_{1/2}$ was calculated from 50 to 70 s during the slow phase of the kinetics.

Cyclic voltammetry. The cyclic voltammetry (CV) experiments were performed on an Autolab PGSTAT302N potentiostat controlled with General Purpose Electrochemical System (GPES) version 4.9, Eco Chemie B. V. Ultrecht, The Netherlands. A three-electrode setup was used that consisted of a glassy carbon disk (3 mm diameter) as the working electrode, a saturated calomel electrode as the reference electrode, and a platinum wire as the counter electrode in an argon-flushed 2 mL cell. The working electrode was polished before each measurement on a red disk NAP (Struers) with 1 µM AP-A suspension and then a 0.3 µM AP-A suspension. The sample solutions were degassed for 3 min for each measurement. The scan rate was 0.1 V s^{-1}. Three scans were realized for each experiment; only the first scan is shown in the figures.

Supplementary Materials: The following supporting information are available online at: https://www.mdpi.com/article/10.3390/molecules27227903/s1, ATCUN peptide characterizations, Figure S1: Cu^{II} removal from Cu^{II}(Aβ) by P followed by UV-Vis, Figure S2: Cu^{II} removal from Cu^{II}(Aβ) by P followed by X-band EPR, Figure S3: Cyclic voltammograms of Cu(P), Figure S4: Cyclic voltammograms of Cu(P), Figure S5: Kinetics of Cu^{II} removal from Cu^{II}(Aβ), Figure S6: Kinetics of ascorbate consumption induced by copper followed by UV-visible spectroscopy at 265 nm, Figure S7: Kinetics of ascorbate consumption induced by Cu(Aβ) followed by UV-visible spectroscopy at 265 nm starting from Cu^{I}(Aβ).

Author Contributions: Conceptualization, C.E. and C.H.; investigation, M.L.; supervision, K.P.M., C.E. and C.H.; validation, C.E. and C.H.; visualization, M.L.; writing—original draft preparation, C.H.; writing—review and editing, M.L., C.E. and C.H. All authors have read and agreed to the published version of the manuscript.

Funding: This research was funded by ERC aLzINK-StG 638712 (attributed to C.H.) and ANR-20-CE07-0009 Copperation (attributed to C.E.).

Institutional Review Board Statement: Not applicable.

Informed Consent Statement: Not applicable.

Data Availability Statement: Data are available on request from the corresponding author.

Acknowledgments: C.H., K.P.M. and C.E. thank ERC (grant number aLzINK-StG 638712) for funding. M.L., K.P.M., C.E. and C.H. thank ANR-20-CE07-0009 for funding. P. Faller, N. Vitale and M. Okafor (Strasbourg) are acknowledged for their fruitful discussions. L. Ganimède is thanked for his participation in the recording of some ROS and the quenching in the Trp fluorescence experiments.

Conflicts of Interest: The authors declare no conflict of interest.

References

1. Dementia Statistics. Available online: https://www.alzint.org/about/dementia-facts-figures/dementia-statistics/ (accessed on 1 July 2022).
2. Alzheimer's Disease: Facts & Figures. Available online: https://www.brightfocus.org/alzheimers/article/alzheimers-disease-facts-figures (accessed on 1 July 2022).
3. Hampel, H.; Hardy, J.; Blennow, K.; Chen, C.; Perry, G.; Kim, S.H.; Villemagne, V.L.; Aisen, P.; Vendruscolo, M.; Iwatsubo, T.; et al. The Amyloid-β Pathway in Alzheimer's Disease. *Mol. Psychiatry* **2021**, *26*, 5481–5503. [CrossRef] [PubMed]
4. Kametani, F.; Hasegawa, M. Reconsideration of Amyloid Hypothesis and Tau Hypothesis in Alzheimer's Disease. *Front. Neurosci.* **2018**, *12*, 25. [CrossRef] [PubMed]
5. Selkoe, D.J.; Hardy, J. The amyloid hypothesis of Alzheimer's disease at 25 years. *EMBO Mol. Med.* **2016**, *8*, 595–608. [CrossRef] [PubMed]
6. Atrian-Blasco, E.; Gonzalez, P.; Santoro, A.; Alies, B.; Faller, P.; Hureau, C. Cu and Zn coordination to amyloid peptides: From fascinating chemistry to debated pathological relevance. *Coord. Chem. Rev.* **2018**, *375*, 38–55. [CrossRef]
7. Stewart, K.L.; Radford, S.E. Amyloid plaques beyond Aβ: A survey of the diverse modulators of amyloid aggregation. *Biophys. Rev.* **2017**, *9*, 405–419. [CrossRef]
8. Huat, T.J.; Camats-Perna, J.; Newcombe, E.A.; Valmas, N.; Kitazawa, M.; Medeiros, R. Metal Toxicity Links to Alzheimer's Disease and Neuroinflammation. *J. Mol. Biol.* **2019**, *431*, 1843–1868. [CrossRef]
9. Faller, P.; Hureau, C. A bioinorganic view of Alzheimer's disease: When misplaced metal ions (re)direct the electrons to the wrong target? *Chem. A Eur. J.* **2012**, *18*, 15910–15920. [CrossRef]

10. Cheignon, C.; Tomas, M.; Bonnefont-Rousselot, D.; Faller, P.; Hureau, C.; Collin, F. Oxidative stress and the amyloid beta peptide in Alzheimer's Disease. *Redox Biol.* **2018**, *14*, 450–464. [CrossRef]
11. Tassone, G.; Kola, A.; Valensin, D.; Pozzi, C. Dynamic Interplay between Copper Toxicity Mitochondrial Dysfunction in Alzheimer's Disease. *Life* **2021**, *11*, 386. [CrossRef]
12. Hureau, C. Chapter 7 Role of Metal Ions in Alzheimer's Disease: Mechanistic Aspects Contributing to Neurotoxicity. In *Alzheimer's Disease: Recent Findings in Pathophysiology, Diagnostic and Therapeutic Modalities*; Govindaraju, T., Ed.; The Royal Society of Chemistry: London, UK, 2022; pp. 170–192.
13. Pedersen, J.T.; Chen, S.W.; Borg, C.B.; Ness, S.; Bahl, J.M.; Heegaard, N.H.; Dobson, C.M.; Hemmingsen, L.; Cremades, N.; Teilum, K. Amyloid-β and α-Synuclein Decrease the Level of Metal-Catalyzed Reactive Oxygen Species by Radical Scavenging and Redox Silencing. *J. Am. Chem. Soc.* **2016**, *138*, 3966–3969. [CrossRef]
14. Cheignon, C.; Jones, M.; Atrian-Blasco, E.; Kieffer, I.; Faller, P.; Collin, F.; Hureau, C. Identification of key structural features of the elusive Cu–Ab complex that generates ROS in Alzheimer's disease. *Chem. Sci.* **2017**, *8*, 5107–5118. [CrossRef] [PubMed]
15. Singh, S.K.; Balendra, V.; Obaid, A.A.; Esposto, J.; Tikhonova, M.A.; Gautam, N.K.; Poeggeler, B. Copper-mediated β-amyloid toxicity and its chelation therapy in Alzheimer's disease. *Metallomics* **2022**, *14*, mfac018. [CrossRef] [PubMed]
16. Fasae, K.D.; Abolaji, A.O.; Faloye, T.R.; Odunsi, A.Y.; Oyetayo, B.O.; Enya, J.I.; Rotimi, J.A.; Akinyemi, R.O.; Whitworth, A.J.; Aschner, M. Metallobiology and therapeutic chelation of biometals (copper, zinc and iron) in Alzheimer's disease: Limitations, and current and future perspectives. *J. Trace Elem. Med. Biol.* **2021**, *67*, 126779. [CrossRef] [PubMed]
17. Gromadzka, G.; Tarnacka, B.; Flaga, A.; Adamczyk, A. Copper Dyshomeostasis in Neurodegenerative Diseases-Therapeutic Implications. *Int. J. Mol. Sci.* **2020**, *21*, 9259. [CrossRef]
18. Ejaz, H.W.; Wang, W.; Lang, M. Copper Toxicity Links to Pathogenesis of Alzheimer's Disease and Therapeutics Approaches. *Int. J. Mol. Sci.* **2020**, *21*, 7660. [CrossRef]
19. Hureau, C. Metal Ions and Complexes in Alzheimer's Disease: From Fundamental to Therapeutic Perspectives. In *Encyclopedia of Inorganic and Bioinorganic Chemistry*; Scott, R.A., Ed.; John Wiley & Sons: Hoboken, NJ, USA, 2019; pp. 1–14.
20. Savelieff, M.G.; Nam, G.; Kang, J.; Lee, H.J.; Lee, M.; Lim, M.H. Development of Multifunctional Molecules as Potential Therapeutic Candidates for Alzheimer's Disease, Parkinson's Disease, and Amyotrophic Lateral Sclerosis in the Last Decade. *Chem. Rev.* **2019**, *119*, 1221–1322. [CrossRef]
21. Migliorini, C.; Porciatti, E.; Luczkowski, M.; Valensin, D. Structural characterization of Cu2+, Ni2+ and Zn2+ binding sites of model peptides associated with neurodegenerative diseases. *Coord. Chem. Rev.* **2012**, *256*, 352–368. [CrossRef]
22. Hureau, C. Coordination of redox active metal ions to the APP and to the amyloid-b peptides involved in AD. Part 1: An overview. *Coord. Chem. Rev.* **2012**, *256*, 2164–2174. [CrossRef]
23. Hureau, C.; Dorlet, P. Coordination of redox active metal ions to the APP protein and to the amyloid-β peptides involved in Alzheimer disease. Part 2: How Cu(II) binding sites depend on changes in the Aβ sequences. *Coord. Chem. Rev.* **2012**, *256*, 2175–2187. [CrossRef]
24. Alies, B.; Renaglia, E.; Rozga, M.; Bal, W.; Faller, P.; Hureau, C. Cu(II) affinity for the Alzheimer's Peptide: Tyrosine fluorescence studies revisited. *Anal. Chem.* **2013**, *85*, 1501–1508. [CrossRef]
25. De Gregorio, G.; Biasotto, F.; Hecel, A.; Luczkowski, M.; Kozlowski, H.; Valensin, D. Structural analysis of copper(I) interaction with amyloid β peptide. *J. Inorg. Biochem.* **2019**, *195*, 31–38. [CrossRef] [PubMed]
26. Hureau, C.; Balland, V.; Coppel, Y.; Solari, P.L.; Fonda, E.; Faller, P. Importance of dynamical processes in the coordination chemistry and redox conversion of copper amyloid-β complexes. *J. Biol. Inorg. Chem.* **2009**, *14*, 995–1000. [CrossRef] [PubMed]
27. Alies, B.; Badei, B.; Faller, P.; Hureau, C. Reevaluation of Copper(I) affinity for amyloid-b peptides by competition with Ferrozine, an unusual Copper(I) indicator. *Chem. A Eur. J.* **2012**, *18*, 1161–1167. [CrossRef] [PubMed]
28. Xiao, Z.; Gottschlich, L.; van der Meulen, R.; Udagedara, S.R.; Wedd, A.G. Evaluation of quantitative probes for weaker Cu(i) binding sites completes a set of four capable of detecting Cu(i) affinities from nanomolar to attomolar. *Metallomics* **2013**, *5*, 501–513. [CrossRef]
29. Alies, B.; Conte-Daban, A.; Sayen, S.; Collin, F.; Kieffer, I.; Guillon, E.; Faller, P.; Hureau, C. Zinc(II) Binding Site to the Amyloid-β Peptide: Insights from Spectroscopic Studies with a Wide Series of Modified Peptides. *Inorg. Chem.* **2016**, *55*, 10499–10509. [CrossRef]
30. Zawisza, I.; Rozga, M.; Bal, W. Affinity of peptides (Aβ, APP, α-synuclein, PrP) for metal ions (Cu, Zn). *Coord. Chem. Rev.* **2012**, *256*, 2297–2307. [CrossRef]
31. Noël, S.; Bustos, S.; Sayen, S.; Guillon, E.; Faller, P.; Hureau, C. Use of a new water-soluble Zn sensor to determine Zn affinity for the amyloid-β peptide and relevant mutants. *Metallomics* **2014**, *6*, 1220–1222. [CrossRef]
32. Esmieu, C.; Guettas, D.; Conte-Daban, A.; Sabater, L.; Faller, P.; Hureau, C. Copper-Targeting Approaches in Alzheimer's Disease: How To Improve the Fallouts Obtained from in Vitro Studies. *Inorg. Chem.* **2019**, *58*, 13509–13527. [CrossRef]
33. Zhou, X.; Smith, Q.R.; Liu, X. Brain penetrating peptides and peptide–drug conjugates to overcome the blood–brain barrier and target CNS diseases. *WIREs Nanomed. Nanobiotechnol.* **2021**, *13*, e1695. [CrossRef]
34. Reissmann, S.; Filatova, M.P. New generation of cell-penetrating peptides: Functionality and potential clinical application. *J. Pept. Sci.* **2021**, *27*, e3300. [CrossRef]
35. Maiti, B.K.; Govil, N.; Kundu, T.; Moura, J.J.G. Designed Metal-ATCUN Derivatives: Redox- and Non-redox-Based Applications Relevant for Chemistry, Biology, and Medicine. *iScience* **2020**, *23*, 101792. [CrossRef] [PubMed]

36. Gonzalez, P.; Bossak, K.; Stefaniak, E.; Hureau, C.; Raibaut, L.; Bal, W.; Faller, P. N-terminal Cu Binding Motifs Xxx-Zzz-His (ATCUN) and Xxx-His and their derivatives: Chemistry, Biology and Medicinal Applications. *Chem. A Eur. J.* **2018**, *24*, 8029–8041. [CrossRef] [PubMed]
37. Harford, C.; Sarkar, B. Amino Terminal Cu(II)- and Ni(II)-Binding (ATCUN) Motif of Proteins and Peptides: MetalBindi ng, DNA Cleavage, and Other Properties. *Acc. Chem. Res.* **1997**, *30*, 123–130. [CrossRef]
38. Bal, W.; Sokołowska, M.; Kurowska, E.; Faller, P. Binding of transition metal ions to albumin: Sites, affinities and rates. *Biochim. Biophys. Acta* **2013**, *1830*, 5444–5455. [CrossRef]
39. Hureau, C.; Eury, H.; Guillot, R.; Bijani, C.; Sayen, S.; Solari, P.L.; Guillon, E.; Faller, P.; Dorlet, P. X-ray and solution structures of CuGHK and CuDAHK complexes. Influence on their redox properties. *Chem. A Eur. J.* **2011**, *17*, 10151–10160. [CrossRef]
40. Hu, X.; Zhang, Q.; Wang, W.; Yuan, Z.; Zhu, X.; Chen, B.; Chen, X. Tripeptide GGH as the Inhibitor of Copper-Amyloid-β-Mediated Redox Reaction and Toxicity. *ACS Chem. Neurosci.* **2016**, *7*, 1255–1263. [CrossRef]
41. Caballero, A.B.; Terol-Ordaz, L.; Espargaró, A.; Vázquez, G.; Nicolás, E.; Sabaté, R.; Gamez, P. Histidine-Rich Oligopeptides To Lessen Copper-Mediated Amyloid-β Toxicity. *Chem. A Eur. J.* **2016**, *22*, 7268–7280. [CrossRef]
42. Esmieu, C.; Ferrand, G.; Borghesani, V.; Hureau, C. Impact of N-Truncated Aβ Peptides on Cu- and Cu(Aβ)-Generated ROS: CuI Matters! *Chem. A Eur. J.* **2021**, *27*, 1777–1786. [CrossRef]
43. Jensen, M.; Canning, A.; Chiha, S.; Bouquerel, P.; Pedersen, J.T.; Østergaard, J.; Cuvillier, O.; Sasaki, I.; Hureau, C.; Faller, P. Bi-functional peptide with β-sheet breaker and chelator moieties against Cu- amyloid-β. *Chem. A Eur. J.* **2012**, *18*, 4836–4839. [CrossRef]
44. Meng, J.; Zhang, H.; Dong, X.; Liu, F.; Sun, Y. RTHLVFFARK-NH2: A potent and selective modulator on Cu2+-mediated amyloid-β protein aggregation and cytotoxicity. *J. Inorg. Biochem.* **2018**, *181*, 56–64. [CrossRef]
45. Perrone, L.; Mothes, E.; Vignes, M.; Mockel, A.; Figueroa, C.; Miquel, M.C.; Maddelein, M.L.; Faller, P. Copper transfer from Cu-Abeta to human serum albumin inhibits aggregation, radical production and reduces Abeta toxicity. *ChemBioChem* **2010**, *11*, 110–118. [CrossRef] [PubMed]
46. Gonzalez, P.; Sabater, L.; Mathieu, E.; Faller, P.; Hureau, C.S. Why the Ala-His-His Peptide Is an Appropriate Scaffold to Remove Redox Silence Copper Ions from the, Alzheimer's-Related, Abeta Peptide. *Biomolecules* **2022**, *12*, 1327. [CrossRef]
47. Rice, M.E. Ascorbate regulation and its neuroprotective role in the brain. *Trends Neurosci.* **2000**, *23*, 209–216. [CrossRef]
48. Harrison, F.E.; May, J.M. Vitamin C function in the brain: Vital role of the ascorbate transporter SVCT2. *Free Radic. Biol. Med.* **2009**, *46*, 719–730. [CrossRef] [PubMed]
49. Conte-Daban, A.; Beyler, M.; Tripier, R.; Hureau, C. Kinetic is crucial when targeting copper ions to fight Alzheimer's disease: An illustration with azamacrocyclic ligands. *Chem. A Eur. J.* **2018**, *24*, 8447–8452, Correction in **2018**, *24*, 13058–13058. [CrossRef]
50. Mena, S.; Mirats, A.; Caballero, A.B.; Guirado, G.; Barrios, L.A.; Teat, S.J.; Rodriguez-Santiago, L.; Sodupe, M.; Gamez, P. Drastic Effect of the Peptide Sequence on the Copper-Binding Properties of Tripeptides and the Electrochemical Behaviour of Their Copper(II) Complexes. *Chem. A Eur. J.* **2018**, *24*, 5153–5162. [CrossRef]
51. Gonzalez, P.; Vileno, B.; Bossak, K.; El Khoury, Y.; Hellwig, P.; Bal, W.; Hureau, C.; Faller, P. Cu(II)-binding to the peptide Ala-His-His, a chimera of the canonical Cu(II)-binding motifs Xxx-His and Xxx-Zzz-His (ATCUN). *Inorg. Chem.* **2017**, *56*, 14870–14879. [CrossRef] [PubMed]
52. Kirsipuu, T.; Zadorožnaja, A.; Smirnova, J.; Friedemann, M.; Plitz, T.; Tõugu, V.; Palumaa, P. Copper(II)-binding equilibria in human blood. *Sci. Rep.* **2020**, *10*, 5686. [CrossRef]
53. Rozga, M.; Sokolowska, M.; Protas, A.M.; Bal, W. Human serum albumin coordinates Cu(II) at its N-terminal binding site with 1 pM affinity. *J. Biol. Inorg. Chem.* **2007**, *12*, 913–918. [CrossRef]
54. Beuning, C.N.; Zocchi, L.J.; Malikidogo, K.P.; Esmieu, C.; Dorlet, P.; Crans, D.C.; Hureau, C. Measurement of Interpeptidic CuII Exchange Rate Constants of CuII-Amyloid-β Complexes to Small Peptide Motifs by Tryptophan Fluorescence Quenching. *Inorg. Chem.* **2021**, *60*, 7650–7659. [CrossRef]
55. Beuning, C.N.; Mestre-Voegtlé, B.; Faller, P.; Hureau, C.; Crans, D.C. Measurement of Interpeptidic Cu(II) Exchange Rate Constants by Static Fluorescence Quenching of Tryptophan. *Inorg. Chem.* **2018**, *57*, 4791–4794. [CrossRef]
56. Heinrich, J.; Bossak-Ahmad, K.; Riisom, M.; Haeri, H.H.; Steel, T.R.; Hergl, V.; Langhans, A.; Schattschneider, C.; Barrera, J.; Jamieson, S.M.F.; et al. Incorporation of β-Alanine in Cu(II) ATCUN Peptide Complexes Increases ROS Levels, DNA Cleavage and Antiproliferative Activity**. *Chem. A Eur. J.* **2021**, *27*, 18093–18102. [CrossRef] [PubMed]
57. Miyamoto, T.; Fukino, Y.; Kamino, S.; Ueda, M.; Enomoto, S. Enhanced stability of Cu2+–ATCUN complexes under physiologically relevant conditions by insertion of structurally bulky and hydrophobic amino acid residues into the ATCUN motif. *Dalton Trans.* **2016**, *45*, 9436–9445. [CrossRef] [PubMed]
58. Gonzalez, P.; Bossak-Ahmad, K.; Vileno, B.; Wezynfeld, N.E.; El Khoury, Y.; Hellwig, P.; Hureau, C.; Bal, W.; Faller, P. Triggering Cu-coordination change in Cu(ii)-Ala-His-His by external ligands. *Chem. Commun.* **2019**, *55*, 8110–8113. [CrossRef] [PubMed]
59. Mital, M.; Wezynfeld, N.E.; Frączyk, T.; Wiloch, M.Z.; Wawrzyniak, U.E.; Bonna, A.; Tumpach, C.; Barnham, K.J.; Haigh, C.L.; Bal, W.; et al. A Functional Role for Aβ in Metal Homeostasis? N-Truncation and High-Affinity Copper Binding. *Angew. Chem. Int. Ed.* **2015**, *54*, 10460–10464. [CrossRef]
60. Wezynfeld, N.E.; Tobolska, A.; Mital, M.; Wawrzyniak, U.E.; Wiloch, M.Z.; Płonka, D.; Bossak-Ahmad, K.; Wróblewski, W.; Bal, W. Aβ5–x Peptides: N-Terminal Truncation Yields Tunable Cu(II) Complexes. *Inorg. Chem.* **2020**, *59*, 14000–14011. [CrossRef]

61. Hureau, C.; Mathé, C.; Faller, P.; Mattioli, T.A.; Dorlet, P. Folding of the prion peptide GGGTHSQW around the copper(II) ion: Identifying the oxygen donor ligand at neutral pH and probing the proximity of the tryptophan residue to the copper ion. *J. Biol. Inorg. Chem.* **2008**, *13*, 1055–1064. [CrossRef]
62. Tobolska, A.; Wezynfeld, N.E.; Wawrzyniak, U.E.; Bal, W.; Wróblewski, W. Copper(ii) complex of N-truncated amyloid-β peptide bearing a His-2 motif as a potential receptor for phosphate anions. *Dalton Trans.* **2021**, *50*, 2726–2730. [CrossRef]
63. Kotuniak, R.; Strampraad, M.J.F.; Bossak-Ahmad, K.; Wawrzyniak, U.E.; Ufnalska, I.; Hagedoorn, P.-L.; Bal, W. Key Intermediate Species Reveal the Copper(II)-Exchange Pathway in Biorelevant ATCUN/NTS Complexes. *Angew. Chem. Int. Ed.* **2020**, *59*, 11234–11239. [CrossRef] [PubMed]
64. Kotuniak, R.; Bal, W. Kinetics of Cu(ii) complexation by ATCUN/NTS and related peptides: A gold mine of novel ideas for copper biology. *Dalton Trans.* **2022**, *51*, 14–26. [CrossRef]
65. Teng, X.; Stefaniak, E.; Girvan, P.; Kotuniak, R.; Płonka, D.; Bal, W.; Ying, L. Hierarchical binding of copperII to N-truncated Aβ4–16 peptide. *Metallomics* **2020**, *12*, 470–473. [CrossRef]
66. Alies, B.; Sasaki, I.; Proux, O.; Sayen, S.; Guillon, E.; Faller, P.; Hureau, C. Zn impacts Cu coordination to Amyloid-ß, the Alzheimer's peptide, but not the ROS production and the associated cell toxicity. *Chem. Commun.* **2013**, *49*, 1214–1216. [CrossRef] [PubMed]
67. Conte-Daban, A.; Day, A.; Faller, P.; Hureau, C. How Zn can impede Cu detoxification by chelating agents in Alzheimer's disease: A proof-of-concept study. *Dalton Trans.* **2016**, *45*, 15671–15678. [CrossRef]
68. Atrian-Blasco, E.; Cerrada, E.; Conte-Daban, A.; Testemale, D.; Faller, P.; Laguna, M.; Hureau, C. Copper(I) targeting in the Alzheimer's disease context: A first example using the biocompatible PTA ligand. *Metallomics* **2015**, *7*, 1229–1232. [CrossRef] [PubMed]
69. Cheignon, C.; Collin, F.; Faller, P.; Hureau, C. Is ascorbate Dr Jekyll or Mr Hyde in the Cu(Aβ) mediated oxidative stress linked to Alzheimer's Disease? *Dalton Trans.* **2016**, *45*, 12627–12631. [CrossRef] [PubMed]
70. Santoro, A.; Walke, G.; Vileno, B.; Kulkarni, P.P.; Raibaut, L.; Faller, P. Low catalytic activity of the Cu(ii)-binding motif (Xxx-Zzz-His; ATCUN) in reactive oxygen species production and inhibition by the Cu(i)-chelator BCS. *Chem. Commun.* **2018**, *54*, 11945–11948. [CrossRef]
71. Magrì, A.; Tabbì, G.; Naletova, I.; Attanasio, F.; Arena, G.; Rizzarelli, E. A Deeper Insight in Metal Binding to the hCtr1 N-terminus Fragment: Affinity, Speciation and Binding Mode of Binuclear Cu2+ and Mononuclear Ag+ Complex Species. *Int. J. Mol. Sci.* **2022**, *23*, 2929. [CrossRef]
72. Zhang, W.; Huang, D.; Huang, M.; Huang, J.; Wang, D.; Liu, X.; Nguyen, M.; Vendier, L.; Mazères, S.; Robert, A.; et al. Preparation of Tetradentate Copper Chelators as Potential Anti-Alzheimer Agents. *ChemMedChem* **2018**, *13*, 684–704. [CrossRef]
73. Pushie, M.J.; Stefaniak, E.; Sendzik, M.R.; Sokaras, D.; Kroll, T.; Haas, K.L. Using N-Terminal Coordination of Cu(II) and Ni(II) to Isolate the Coordination Environment of Cu(I) and Cu(II) Bound to His13 and His14 in Amyloid-β(4-16). *Inorg. Chem.* **2019**, *58*, 15138–15154. [CrossRef]
74. Ipsen, J.Ø.; Hallas-Møller, M.; Brander, S.; Lo Leggio, L.; Johansen, K.S. Lytic polysaccharide monooxygenases and other histidine-brace copper proteins: Structure, oxygen activation and biotechnological applications. *Biochem. Soc. Trans.* **2021**, *49*, 531–540. [CrossRef] [PubMed]
75. Chan, W.W.P. (Ed.) *Fmoc Solid Phase Peptide Synthesis: A Practical Approach*; Oxford University Press: Oxford, UK, 1999.